THE ASTROPHYSICAL JOURNAL, Vol. 157, August 1969

NEW EVIDENCE FOR THE OBLIQUE-ROTATOR MODEL FOR α^2 CANUM VENATICORUM*

K. KODAIRA† AND W. UNNO‡
Mount Wilson and Palomar Observatories, Carnegie Institution of Washington,
California Institute of Technology
Received December 16, 1968

ABSTRACT

We have reexamined the oblique-rotator hypothesis for this spectrum variable. Profiles of Si II λλ4128 and 4130 were measured on polarimetric, high-dispersion spectra (1.5 Å mm^{-1}, four polarization components) of α^2 CVn. We determine the position angle of the line of force of the effective magnetic field α as well as the strength of the effective longitudinal magnetic field H^*. The observed H^*-curve differs slightly in form from that of Babcock and Burd but is in general agreement. Two possible solutions were obtained for the α-curve. One of them was found to show the rotatory behavior consistent with the observed H^*-curve and also with the oblique-rotator model proposed by Böhm-Vitense. Strong variations of the profiles of Eu II λ4129, Cr II λ4555, and λ4559 were observed. They coincided well with the predictions given by Böhm-Vitense for her model, suggesting again the validity of the oblique-rotator hypothesis for α^2 CVn.

I. INTRODUCTION

The star α^2 CVn is a bright, spectrum-variable star (Ap, $V = 2.9$ mag, Eu-Cr type, regular variable) whose variability was found by Ludendorff (1906). As studied later, quantitatively, by Burbidge and Burbidge (1955), groups of lines typified by Eu II and Cr II undergo large variations in intensity with opposite phase while lines of Si II and Mg II remain nearly constant. Following the early fundamental studies, Farnsworth (1932) determined the time of maximum intensity of Eu II lines by investigating low-dispersion spectrograms. Her formula,

$$\text{J.D.} = 2419869.720 + 5.46939E\,, \qquad (1)$$

was adopted by other investigators and will also be used in the present paper.

Struve and Swings (1943) identified the absorption lines and showed that the radial velocities of different elements vary in different ways, corresponding to those of the intensity variation. The radial velocity of Eu II lines ranges from -9 km sec^{-1} at $E = 0.8$ to $+20$ km sec^{-1} at $E = 0.3$, that of Cr II lines ranges from -13 km sec^{-1} at $E = 0.1$ to $+9$ km sec^{-1} at $E = 0.9$, and Si II and Mg II lines show hardly any variation in radial velocity.

Babcock and Burd (1952) succeeded in determining the strength of the effective longitudinal magnetic field of this star. They measured the Zeeman effects on high-contrast spectrograms with a dispersion of 4.5 Å mm^{-1}, using the double circular analyzer. The measured field strength reached the maximum of about $+1.6$ kgauss near $E = 0.5$ and remained around -1 kgauss for $0.8 \lesssim E \lesssim 1.2$. At the phases $E \simeq 0.3$ and $\simeq 0.7$, where the polarity of the field changes, a "crossover effect" was observed in some lines.

Böhm-Vitense (1966) proposed an oblique-rotator model for α^2 CVn, which was con-

* This research was supported in part by the U.S. Air Force under grant AFOSR 68-1401, monitored by the Air Force Office of Scientific Research of the Office of Aerospace Research.

† On leave from Tokyo Observatory, University of Tokyo.

‡ Department of Astronomy, University of Tokyo.

sistent in many aspects with the above data and which predicted a strong variation in the profiles of Eu II and Cr II and Cr II lines.

Additional observations giving new physical data are required, to provide a choice among the various hypotheses. We present here spectrographic observations of the transverse and longitudinal Zeeman effects, and of the variation of line profiles of α^2 CVn. The results are discussed to support the oblique-rotator hypothesis.

II. THEORETICAL BACKGROUND

One of us (Unno 1956) studied the problem of radiation transfer in a line split in the normal Zeeman pattern, making use of the Stokes parameters $I = (I,Q,U,V)$. According to his solution,

$$r_I \equiv \frac{I_0(0,\theta) - I(0,\theta)}{I_0(0,\theta)} = \frac{\beta_0 \cos\theta}{1 + \beta_0 \cos\theta}\left[1 - \frac{1 + \eta_I}{(1 + \eta_I)^2 - \eta_Q^2 - \eta_V^2}\right], \tag{2a}$$

$$r_Q \equiv \frac{Q_0(0,\theta) - Q(0,\theta)}{I_0(0,\theta)} = \frac{\beta_0 \cos\theta}{1 + \beta_0 \cos\theta}\frac{\eta_Q}{(1 + \eta_I)^2 - \eta_Q^2 - \eta_V^2}, \tag{2b}$$

$$r_V \equiv \frac{V_0(0,\theta) - V(0,\theta)}{I_0(0,\theta)} = \frac{\beta_0 \cos\theta}{1 + \beta_0 \cos\theta}\frac{\eta_V}{(1 + \eta_I)^2 - \eta_Q^2 - \eta_V^2}, \tag{2c}$$

$$(U \equiv 0), \tag{2d}$$

where the subscript 0 refers to the continuous radiation; β_0 is the linear coefficient in the approximate source function $B = B_0(1 + \beta_0\tau)$; and η_I, η_Q, and η_V are absorption coefficients expressed as

$$\eta_I = \frac{\eta_p}{2}\sin^2\Psi + \frac{\eta_l + \eta_r}{4}(1 + \cos^2\psi), \tag{3a}$$

$$\eta_Q = \left(\frac{\eta_p}{2} - \frac{\eta_l + \eta_r}{4}\right)\sin^2\psi, \quad \text{and} \tag{3b}$$

$$\eta_V = \frac{-\eta_l + \eta_r}{2}\cos\psi, \tag{3c}$$

where ψ is the angle between the line of force and the line of sight, and η_p, η_l, and η_r denote the ratios of the line absorption coefficients to the continuous absorption coefficient for the π-component, the left-circular σ-component, and the right-circular σ-component, respectively. The computation for arbitrary Zeeman patterns by Stepanov (1960) gave essentially the same results.

When we observe line profiles through an analyzing double-image prism, we obtain two profiles, $r_{X,0}$ and $r_{Y,0}$, where X is the ordinary and Y the extraordinary ray and where the second subscript denotes the phase shift (see below). These are related to the theoretical quantities above by

$$r_{Y,0} - r_{X,0} = 2r_Q \sin 2\Phi. \tag{4a}$$

Here Φ is the azimuthal angle of the line of force with respect to the optical device. When we set a $\lambda/4$ plate before the double-image prism with an angle of $\pi/4$ between the axes, we obtain line profiles $r_{X,\pi/2}$ and $r_{Y,\pi/2}$, which have the following relation with r_V:

$$r_{X,\pi/2} - r_{Y,\pi/2} = 2r_V. \tag{4b}$$

In both cases, the average of the two profiles equals r_I:

$$2r_I = r_{X,0} + r_{Y,0} = r_{X,\pi/2} + r_{Y,\pi/2} . \quad (4c)$$

The different axes and angles are illustrated in Figures 1 and 2.

In principle one can derive the three-dimensional effective magnetic field from the observation of the line profiles $r_{X,0}$, $r_{Y,0}$, $r_{X,\pi/2}$, and $r_{Y,\pi/2}$ (only three of these four are strictly independent), and this method was successfully applied to studies of the magnetic field in sunspots (Nishi 1962). In the above calculation, it is assumed that the magnetic field and the absorption coefficients are constant throughout the atmosphere in any specific region of the stellar disk. Nevertheless, in applying this fundamental theory to the study of α^2 CVn, one encounters some difficulties. When observing line

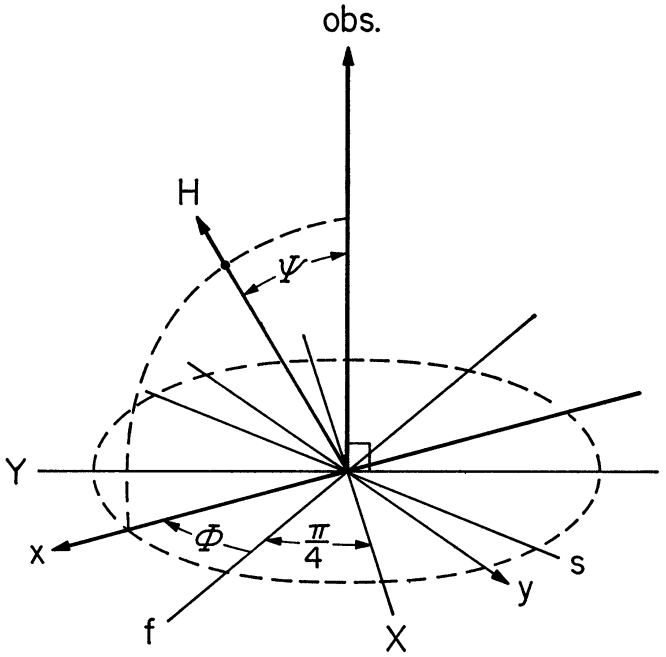

FIG. 1.—Definition of angles. *Obs*, line of sight; *H*, line of force of the magnetic field; *X Y*, axes of the analyzing double-image prism; *fs*, axes of the λ/4 plate. *X Y* and *fs* are telescopic images on the celestial sphere.

profiles integrated all over the stellar disk, one can determine only mean values not only weighted by surface brightness, $\beta_0 \cos\theta/(1 + \beta_0 \cos\theta)$, but also depending on the distribution of the absorbing elements and of quantities concerning the magnetic field. Further, the effect of rotation, coupled with that of a probably inhomogeneous distribution, influences the line profiles, making the reduction of the observed data very difficult.

This situation has forced investigators to determine only the so-called effective field strength, equating the shifts of the centers of gravity of the lines $r_{X,\pi/2}$ and $r_{Y,\pi/2}$ to the normal Zeeman shifts (see Babcock 1962). The measured quantity is related to the field strength, H, mainly coupled with a factor $\cos\psi$, as seen in equation (3c). It is, however, astonishing that the "effective" field strengths derived by Babcock and Burd (1952) from different elements, even from Cr II and Eu II, show only small scatter, although the distributions of Cr II and of Eu II over the stellar surface seem to complement each other. Böhm-Vitense (1965) reached the same conclusion in her theoretical study, based on specific models. This can be interpreted in terms of the dominant effect of the projection of a spherical surface onto a disk. This, enhanced by the rotation and limb darken-

ing, gives most weight to the disk center in the measurement of the center of gravity of a line. It is here assumed that the actual mean field strength does not vary in order of magnitude from one hemisphere to another.

In contrast to the inclination angle ψ, the azimuthal angle Φ appears only on the right-hand term of equation (4a). From a single observation of $(r_{Y,0} - r_{X,0})$ one cannot separate sin 2Φ from other factors. The position angle α of the effective transversal field (referred to the equatorial coordinate), however, can be determined when one rotates the axes of the polarimetric devices or the stellar image in order to vary the angle Φ continuously. The maximum response in $\delta r = (r_{Y,0} - r_{X,0})$ corresponds to sin $2\Phi = 1$, i.e.,

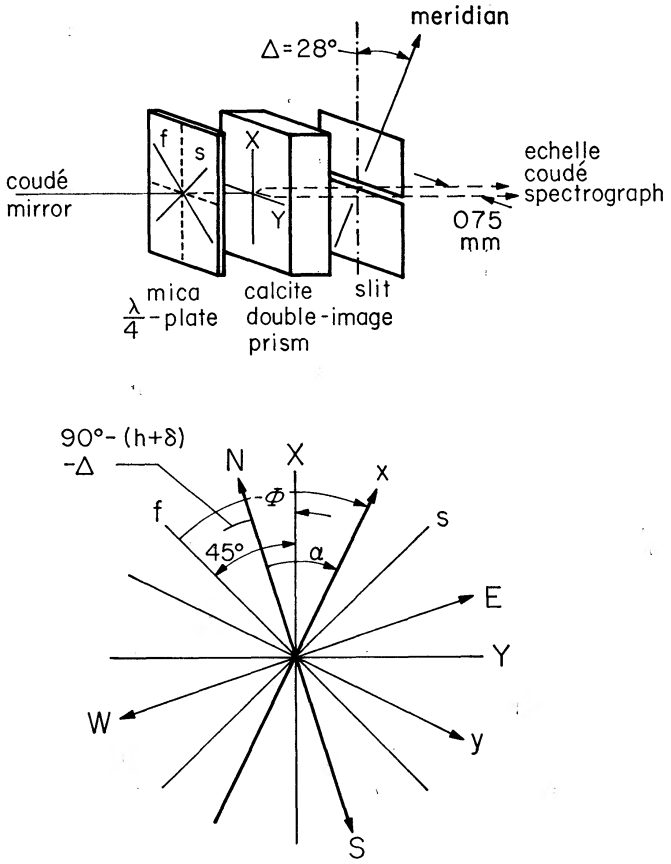

FIG. 2.—Analyzing optical device and relevant angles. *fs*, axes of the λ/4 plate; *XY*, axes of the double-image prism; *x*, see Fig. 1. *xy* and NESW are telescopic images on the slit surface of the coudé spectrograph (telescope west). h = hour angle, δ = declination, Δ = slit rotation for echelle system.

$\Phi = \pi/4 \pm n\pi$, and the position angle of the Y-axis is then the position angle of the effective transversal magnetic field (see Fig. 2). In spectrographic observations, the rotation cannot be continuous; nevertheless, the position angle α can be determined by the same principle, as demonstrated in § IV. If the response δr could be measured accurately for several different angles Φ, it would be possible to determine further the strength of the effective transversal field. This is, however, not the case for α^2 CVn because of the rotational effect and the lack of sufficient time resolution.

It should still be noted that the effective field determining the position angle α may refer to a region which is different from that determining the strength of the effective longitudinal field. We can, nevertheless, assign the measured α to the measured strength of the effective longitudinal field, if we can assume smoothness of the field over a stellar radius.

III. OBSERVATIONAL TECHNIQUE

The star was observed in March and May of 1967 with the echelle spectrograph at the coudé focus of the 74-inch reflector of the Okayama Astrophysical Observatory. An analyzing double-image prism was set directly in front of the slit of the spectrograph, which separated the ordinary and extraordinary stellar images by about 0.75 mm along the slit. When necessary, a $\lambda/4$ plate was inserted with an angle of $\pi/4$ between the axes of the prism and those of the $\lambda/4$ plate (Fig. 2). The two-component spectra were secured on baked 103a-O plates with a dispersion of 1.5 Å mm^{-1} near Hγ over a range of $\lambda\lambda$3700–4800 Å. In order to compare the separate microphotometer tracings of the spectra taken in the different polarizations on one plate, the comparison iron-arc spectrum was superposed on the stellar spectrum. While this method naturally lost us some information, it did permit us, with careful microphotometer technique, to compare tracings with an accuracy of $\Delta\lambda \approx 0.005$ Å, which corresponds to an error of 0.4 km sec^{-1} in Doppler velocity, or 0.3 kgauss in the strength of the magnetic field.

The polarization device was kept fixed; the stellar image rotated relative to it at the coudé focus. We had originally designed a device to obtain spectra of the four polarization components simultaneously. The required time resolution forced us to take two-component spectra alternating with and without the $\lambda/4$ plate. The angular resolution of Φ is set in our case by the diurnal rotation, or 15 degrees for one hour of exposure. The exposure time was about 15 minutes under the best conditions, and 90 minutes with poor seeing. It turned out that the spectrograph showed no appreciable selective difference in response to the ordinary and the extraordinary rays. Table 1 contains the observational data, i.e., the Julian Day of the observation, the epoch and phase calculated according to equation (1), the hour angle (including the exposure time) and the optical device used.

The optical effects of the coudé system on polarized light were previously studied with and artificial light source on the top of the telescope. As the 74-inch reflector is mounted in the English style, the instrumental polarization arises from two 45° plane coudé mirrors, made of the same material. When we express the incident light with the Stokes parameter $I_0 = (I_0, Q_0, V_0, U_0)$, the emergent light I is written as (cf. Chandrasekhar 1960)

$$I \propto R_1 \cdot A \cdot R_2 \cdot A \cdot I_0 . \tag{5}$$

Here A is the matrix representing the effect of a coudé mirror; the elements of the matrix A are functions of the reflectivities k and the phase shifts ϵ for light polarized in the main plane (subscript $\|$) and in the plane of the mirror surface (subscript $\perp$). The R's are matrices representing the rotations of the coordinate systems; the special matrix R_2 is concerned with the relative position of the two coudé mirrors and depends only on the declination of the star; R_1 contains only the hour angle of the star as variable, when I_0 is referred to the equatorial coordinate and I to the coordinate fixed on the Earth. Combining the effects of the polarizer on the light source and of the analyzer in front of the spectrograph slit, and varying the declination, we determined the parameters

$$\Delta \log k = \frac{k_\perp - k_\|}{k_\perp} , \tag{6a}$$

$$\Delta\epsilon = \epsilon_\perp - \epsilon_\| + \pi . \tag{6b}$$

The photomultiplier system used was also calibrated for differently polarized light. The results found were

$$\Delta \log k = 0.03 \pm 0.03 , \tag{7a}$$

and

$$\Delta\epsilon = 20° \pm 2\overset{\circ}{.}5 \text{ (incident angle } = 45°) . \tag{7b}$$

The results were the same, within the accuracy of measurement, in March and May 1967. The effects of the two coudé mirrors compensate each other for $\delta = 0°$. In the case of α^2 CVn ($\delta = +38°51'$) these cause a mixing of less than 10 percent among the independent components of the polarized light. This result assures us that the influence of the mirror system is small in the following determination of the strength of the effective longitudinal magnetic field and the position angle of the effective transversal field of α^2 CVn.

TABLE 1

OBSERVATIONAL DATA

CE	J D. 2439000+	Epoch, Phase	Hour Angle (degrees)	Note
189	574 09	3602 663	E 26 ± 7 5	λ/4
190	12	669	E 14 ± 2	
191	15	674	E 1 5± 5 5	λ/4
192	.19	682	W 11 ± 4	
193	.22	.686	W 23 5± 6	λ/4
194	.27	696	W 40 ± 7 5	
195	.33	707	W 59 ± 7 5	λ/4
196	97	.824	E 68 ±11	λ/4
197	575 02	834	E 48 ± 4 5	
198	06	.841	E 34 ± 5 5	λ/4
199	.09	846	E 24 ± 2 5	
200	.12	.852	E 13 ± 4	λ/4
201	.16	.859	0 ± 6	
204	576 99	3603 194	E 59 5±12	λ/4
205	577 06	.207	E 34 5±10	
206	11	216	E 15 ± 5 5	λ/4
212	626 03	3612 159	W 5 ± 5	λ/4
213	08	.168	W 21 ± 2	mixed
214	.10	172	W 32 ± 3	
215	14	179	W 46 5± 9	λ/4
218	99	335	E 10 ± 7 5	λ/4
219	627 03	342	W 6 ± 3 5	
220	07	.350	W 23 ± 5 5	λ/4
221	.11	357	W 37 ± 7	
222	628 00	.520	E 1 5±11	λ/4
223	05	.528	W 15 5± 5 5	
224	10	537	W 30 5± 8	λ/4
225	.14	547	W 47 5± 6	
226	97	698	E 13 5± 5 5	λ/4
227	629 01	702	W 1 ± 4	
228	04	710	W 11 5± 4	λ/4
229	629 06	3612 712	W 19 5± 2 5	

IV. OBSERVATIONAL RESULTS

The line profiles of α^2 CVn are much more strongly affected by the rotation (20 km sec^{-1}; 0.3 Å) than by the magnetic field (2 kgauss; 0.03 Å). The rotational effect, coupled with the probable inhomogeneous distribution of chemical elements over the stellar surface, complicate the study of those line profiles whose intensities change remarkably rapidly (see Figs. 5 and 7). Because their radial velocities and intensities are approximately constant throughout their period, the lines of Si II λλ4128 and 4130 were chosen for a study of magnetic effects. These lines show the anomalous Zeeman effect with patterns

$$\lambda 4128: (0.03,0.09)\ 0.77\quad 0.83\ ,\ 0.89\ ,\ 0.94 \qquad (8a)$$

and

$$\lambda 4130: (0.17,0.51,0.86)\ 0.34\ ,\ 0.69\ ,\ 1.03\ ,\ 1.37\ ,\ 1.71\ . \qquad (8b)$$

The weighted mean g-factors z, equivalent to the g-factor of the normal Zeeman pattern, are $z = 0.86$ and $z = 1.02$ for λ4128 and λ4130, respectively.

Figure 3*a* shows examples of measured line profiles $r_{X,\pi/2}$ and $r_{Y,\pi/2}$. For profiles broadened by rotation, it has scarcely any meaning to derive $2r_V = r_{X,/\pi 2} - r_{Y,\pi/2}$ and to compare them with predictions from even a simplified theory. We measure, therefore, the shifts $2\Delta\lambda$ which bring the profiles $r_{Y,\pi/2}$ into the best overlap with the profiles

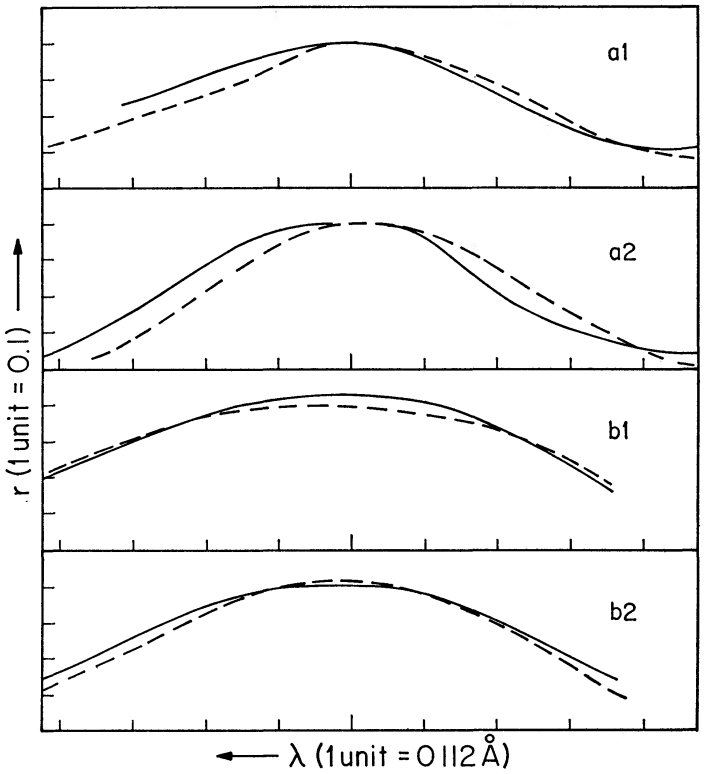

FIG 3.—Examples of microphotometer tracings. *a*1, CE 224 Si II λ4128; *a*2, CE 200 Si II λ4128 (*solid line*, $r_{X,\pi/2}$; *dashed line*, $r_{Y,\pi/2}$). H^* (*a*1) = +2.0 kgauss; H^* (*a*2) = +3.7 kgauss. *b*1, CE 223 Si II λ4130; *b*2, CE 214 Si II λ4130 (*solid line*, $r_{X,0}$; *dashed line*, $r_{Y,0}$). I (*b*1) = −4; I (*b*2) = +2.

$r_{X,\pi/2}$. The strength of the effective longitudinal magnetic field H^* is then defined as follows:

$$\Delta\lambda(\text{Å}) = 4.67 \times 10^{-13}\lambda^2(\text{Å}) \cdot H^* \cdot z = 0.008 H^*(\text{kgauss}) \cdot z\ . \qquad (9)$$

In Table 2, H^*'s are given as the mean of the values derived from λ4128 and λ4130 for every spectrum taken with the λ/4 plate. The maximum error can be as large as ±1 kgauss, which is caused mainly by the difficulty in detecting small shifts of lines with broad flat profiles. The results are also plotted in Figure 4*a* and compared with H_{eff} measured by Babcock and Burd (1952). In spite of the great difficulty of obtaining the measurements, both curves are very similar except for small shifts in phase $\Delta E \approx 0.1$ and in strength $\Delta H \approx 0.5$ kgauss. It would be premature to draw any conclusion from these differences.

Figure 3*b* shows examples of measured line profiles $r_{X,0}$ and $r_{Y,0}$. As shown in the

MEASURED STRENGTH OF THE EFFECTIVE LONGITUDINAL MAGNETIC FIELD

CE	Epoch, Phase 3600+	H^* (kgauss)
189	02 663	+1 29
191	02 674	+0 55
193	02 686	+2 40
195	02 707	+3 50
196	02 824	+1 40
198	02 841	−0 37
200	02 852	+1 85
204	03 194	0
206	03 216	−2 95
212	12 159	+0 55
215	12 179	−2 22
218	12 335	−0 74
220	12 350	−0 18
222	12 520	+2 77
224	12 537	+2 29
226	12 698	0
228	12 710	0

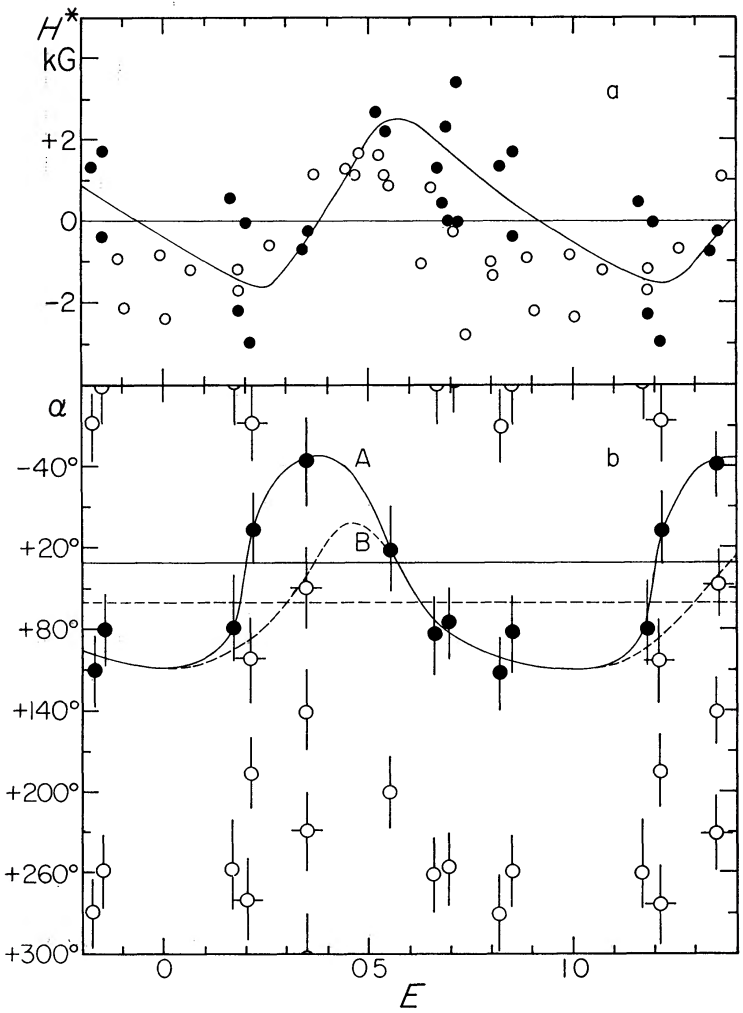

FIG. 4.—Measured strength of the effective longitudinal magnetic field and measured position angle of the effective transversal magnetic field of α^2 CVn. (*a*) Field strength; *filled circles*, present data; *open circles*, Babcock and Burd (1952) H_{eff}(Si II). (*b*) Position angle; symbols represent possible solutions; vertical bars, error limits. *Solid line* and *dashed line:* reasonable variation curves, *A* and *B*.

theoretical study by Unno (1956), the quantity $\delta r = r_{Y,0} - r_{X,0} = 2r_Q \sin 2\Phi$ is related to the difference of the sharpness of the line profile between $r_{Y,0}$ and $r_{X,0}$, and proportional to sin 2Φ for any fixed phase E. The expected maximum value of δr would be about 0.1–0.2 near the line center if the star did not rotate. Because of the large rotational effect in α^2 CVn, one has to expect δr(max) of about 0.04 for the actual case. The accuracy of measurement of r at one point in a profile compares favorably with this value. The difference δr, however, has a greater accuracy because the two profiles are recorded on the same part of a spectrogram and calibrated with the same characteristic curve. We estimate an accuracy of ± 0.01 for the mean value $\langle \delta r \rangle = [\delta r(4128) + \delta r(4130)]/2$. As there is an uncertainty of up to 25 percent of the quantity to be measured, we introduce an "index of difference" I which takes discrete values $0, \pm 1, \pm 2, \ldots$, nearest to $\delta r/0.01$. The index, I^* is finally defined as $[I(4128) + I(4130)]/2$ at the line center and is given in Table 3 for each spectrum taken without a $\lambda/4$ plate. When more than two

TABLE 3

FOR THE DETERMINATION OF THE POSITION ANGLE α

E	CE	h	I^*	k	$\alpha \pm n\pi$
0 17	214	W 32°	+3 0	(3)	81°
21	205	E 34°.5	0	.....	12°.5, 102°.5
.35	219	W 6°	0	.....	46°, 136°
	221	W 37°	0		
.54	223	W 15°.5	−3 0	3 3	20°.5
	225	W 47°.5	0		
.67	190	E 14°	0	2 6	82°
	192	W 11°	+2.0		
.70	194	W 40°	+2 0		
	227	W 1°	0	2 0	70°
	229	W 19°.5	+1.0		
83	197	E 48°	−0 5	(3 7)	112°
0 85	199	E 24°	−1 5	3.7	80°
	201	0°	+1 5		

NOTE —I^*, index of difference; h, hour angle; k, see text.

spectra are available for one phase E, one can determine the position angle of the effective transversal magnetic field $\alpha(E)$ which best satisfies the equations,

$$I_i^* = k(E) \sin 2\Phi_i \qquad -\Phi_i = \alpha(E) + 45° - [90° - (h_i + \delta) - \Delta] = \alpha(E) + h_i + 22°, \tag{10}$$

where h_i denotes the hour angle, δ the declination of α^2 CVn (+39°), and Δ the angle of the rotation of the slit for the echelle system (28°) (see Fig. 2). The coefficient $k(E)$ is essentially related to the strength of the effective transversal field and must be positive, in our definition. At phases $E = 0.35$, 0.54, 0.67, 0.70, and 0.85, where we have two or more observations available, the solutions can be easily obtained. When three observations exist, as at $E = 0.70$, the third observation can also be used to check the consistency; CE 194 and CE 229 lead to a solution $\alpha = +73° \pm n\pi$, and CE 227 to $\alpha = +67° \pm n\pi$. In order to obtain a result from a single observation, one has to assume the value of k. At $E = 0.83$ the value of k at $E = 0.85$ can be safely adopted: $k = 3.7$. In this special case the solution of α is insensitive to the variation of the adopted value of k. At $E = 0.17$ one cannot assume a value of k smaller than 3.0 (unless sin $2\Phi > 1$), which

is nearly the mean value of k determined for phases with more than one observation. Even an extremely large value $k = 5.0$ leads to $\alpha(0.17) = +55° \pm n\pi$, which differs only 26° from $\alpha = 81° \pm n\pi$ obtained for $k = 3.0$. At $E = 0.21$ the formal solution for α does not depend on k because the index of difference I^* is zero. The results are shown in the last two columns of Table 3.

The ambiguity of ± 1 in I^* causes an uncertainty in α of less than 30° except for the cases $E = 0.21$ and $E = 0.35$. At these phases the available indices are all zero, and $\Delta I^* = \pm 1$ corresponds to $\Delta \sin 2\Phi = \pm 1$, making α indefinite if $k \lesssim 1.0$. One has, however, to adopt $k \gtrsim 3$ for $E = 0.21$ because $|H^*|$ reaches its local maximum at this phase while k must be larger than ~ 3 at $E = 0.17$ (see Fig. 4*a*). Consequently, the uncertainty in α is again less than 30° at $E = 0.21$. For $E = 0.35$ the uncertainty remains within $\pm 30°$, corresponding to $\Delta I^* = \pm 1$ insofar as we can assume $k \gtrsim 1.2$. This assumption is consistent with the following discussion and does not introduce any essential limitation on it. Figure 4*b* shows $\alpha(E)$, which are the position angles. Although α has an uncertainty of $\pm n\pi/2$ at $E = 0.21$ and 0.35, and of $\pm n\pi$ at other phases, it is easy to see that the condition of smooth variation allows only two reasonable α-curves (A and B in Fig. 4*b*). It is especially noticeable that the α-curve A has a remarkable phase relation with the observed H^*-curve which suggests the rotatory nature of this star. In the next section, the consistency of the solution A with the oblique-rotator hypothesis will be further discussed.

Although variation of the line profiles is an inevitable conclusion from the oblique-rotator hypothesis for spectrum-variable stars, no systematic effort has hitherto been made to detect this phenomenon. We observed variations of the mean profiles r_I, and examples are illustrated in Figures 5 and 7. The profiles of Si II lines hardly vary, while that of Eu II λ4129, close to and traced together with the Si II lines, shows a spectacular change. When one plots r_I at a certain wavelength in time sequence, one finds that even the small differences among profiles which have been drawn together for approximately the same phase, in Figure 5, are probably real. The equivalent widths of Eu II lines are compared with those measured at lower dispersion by Burbidge and Burbidge (1955) in Figure 6. The differences might be related to that of the H-curve found between ours and that of Babcock and Burd (1952), or to the difference in technique. The observed variations of our profiles of Cr II λλ4555, 4559 and Fe II 4556 are shown in the density tracings in Figure 7, and they are compared in the following section with the theoretical profiles calculated by Böhm-Vitense (1966) for her oblique-rotator model of α^2 CVn.

V. DISCUSSION

In order to explain the complicated phenomena in magnetic or spectrum-variable stars described in § I, various hypotheses have been developed. The oblique-rotator hypothesis mentioned by Babcock (1951) and first applied by Deutsch (1952, 1956, 1958) to comprehensive studies of another magnetic variable star, HD 125248, seems the most applicable to α^2 CVn. Deutsch (1958) showed that the observed variations in line intensities, radial velocities, and strength of the effective longitudinal magnetic field of HD 125248, can be explained if one assumes appropriate distributions of chemical elements and magnetic field over the surface of a star which is rotating around an axis inclined with regard to the line of sight. Recently, Böhm-Vitense (1966, 1967) proposed an oblique-rotator model for α^2 CVn with a nondipole magnetic field consistent with many aspects of the observed properties of this star.

The observational facts verifying the oblique-rotator hypothesis were essentially:

1. The crossover effect: The profiles $r_{X,\pi/2}$ and $r_{Y,\pi/2}$ show a difference in sharpness at the phases when the effective longitudinal magnetic field changes its sign. This phenomenon was reasonably interpreted by Babcock (1956) as the Zeeman-effect pattern altered by the Doppler effect on a rotating magnetic star.

2. The phase relation between line-intensity curve and radial-velocity curve: The phase of maximum intensity occurs when the radial velocity changes its sign from nega-

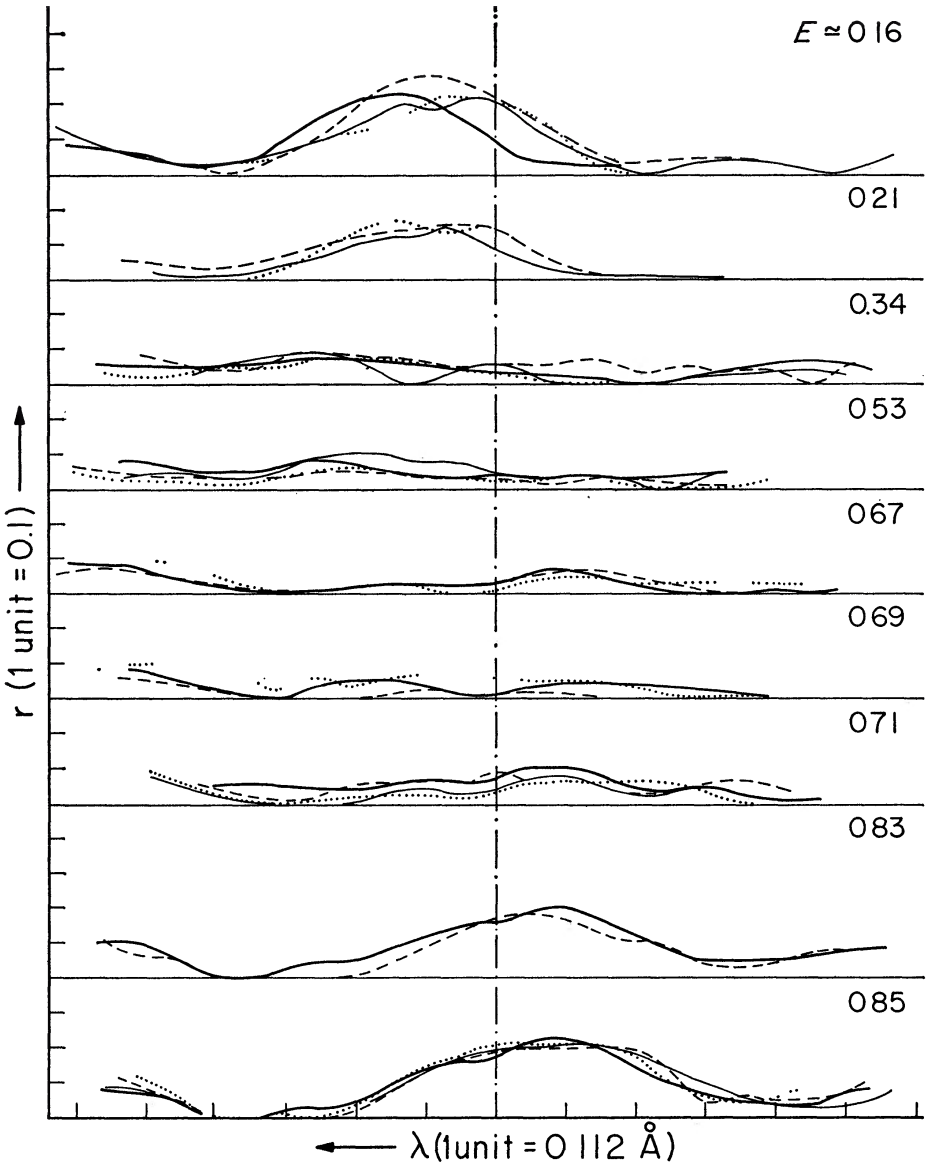

FIG. 5.—Variation of Eu II λ4129. Profiles are shown as intensity curves

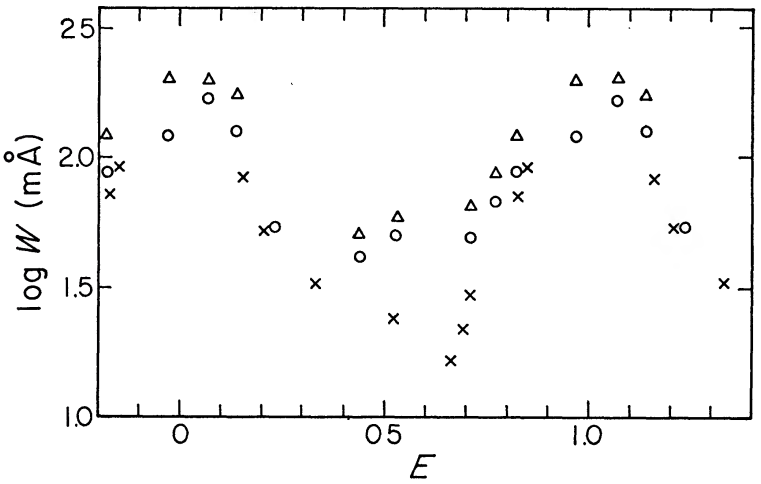

FIG. 6.—Variation of equivalent widths of Eu II lines. *Crosses*, present measurement of λ4129; *open circles* and *triangles*, λ4129 and λ4435 from Burbidge and Burbidge (1955).

tive to positive. This can be easily understood as the central-meridian passage of the center of the effective region rich in a given element. (At minimum intensity, the radial velocity may change from positive to negative, but this is not yet definitely established.)

3. The period-velocity relation: The observed period of the variation is comparable to the travel time around the stellar circumference at a velocity equal to that derived from the observed line width.

These facts concern the motion along the line of sight. Our new data add information concerning motion in a plane perpendicular to the line of sight and accordingly provide a possibility of examining the oblique-rotator hypothesis from a three-dimensional point of view.

As was pointed out in the last section, the α-curve labeled A in Figure 4*b* has a special phase relation with the observed H^*-curve in Figure 4*a:* (*a*) The phases for $H^* \fallingdotseq 0$

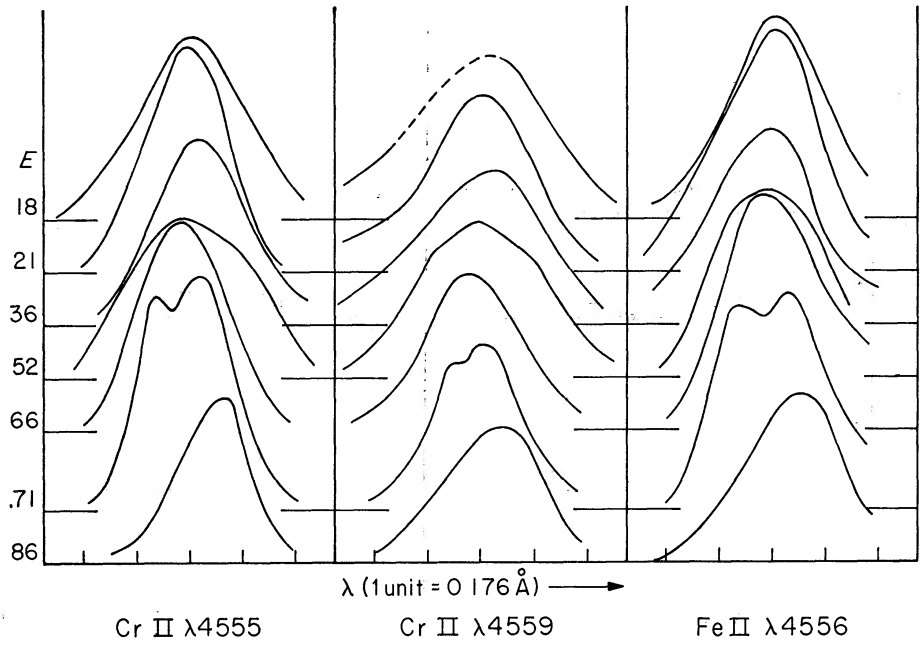

FIG. 7.—Variation of Cr II λλ4555 and 4559, and Fe II λ4556. Profiles are shown as density curves

coincide with the phases for the maximum or the minimum position angle. (*b*) The phases for the maximum or the minimum of H^* coincide with the phases for the mean position angle $\langle a \rangle \fallingdotseq 30°$. These facts strongly suggest the rotational origin of the variation of the magnetic field; the moment (*a*) represents the limb passages of the main magnetic polar regions which provide nearly poloidal field over the stellar surface, and it is in good agreement with the observation of the crossover effect mentioned in (1), above. The point (*b*) represents the central-meridian passage of the main magnetic polar regions, which produces phenomena similar to the effects discussed in (2), above. The actual field of α^2 CVn can hardly be expected to be rigorously poloidal, but can be nearly poloidal because the duration for $\alpha \lesssim \langle \alpha \rangle$ is $\Delta E \fallingdotseq 0.4$ while that for $\alpha \gtrsim \langle \alpha \rangle$ is $\Delta E \fallingdotseq 0.6$, for the probable α-curve solution A. Figure 8 shows schematically the configurations corresponding to these special passages of the magnetic polar regions. The angles which determine the configuration are also shown in Figure 8. In the solution A adopted above, the position angle of the rotational axis ω of α^2 CVn is $\langle \alpha \rangle \fallingdotseq 30°$. The present analysis provides one of the few possibilities of determining the direction of the rotational axis of a single star.

In our picture of a nearly poloidal field, the angle β between the rotational axis ω

and the magnetic axis m, and the angle i between the rotational axis and the line of sight are related to the elongation $p = a - \langle a \rangle$ through

$$\tan p = \frac{\sin \beta \cdot \sin q}{\cos \beta \sin i - \sin \beta \cos i \cos q} . \tag{11}$$

Here q is the rotational angle measured from the central meridian (see Fig. 8). For the phase of maximum or minimum elongation, $p_0 = |a - \langle a \rangle|_{\max}$, the equation,

$$\tan p_0 = \sin \beta [\pm \sin (i + \beta) \sin (i - \beta)]^{-1/2} , \tag{12}$$

must be satisfied. Since the sense of rotation is arbitrary, we set a limit $\pi/2 \geq i$ on i. On the other hand, there is a condition

$$\begin{aligned} &\beta + i > \pi/2 \quad \text{in case} \quad \pi/2 - \beta \geq 0 \\ \text{or} \quad &\beta - i < \pi/2 \quad \text{in case} \quad \pi/2 - \beta < 0 , \end{aligned} \tag{13}$$

because the polarity of the effective longitudinal field changes. The quantity $(\pi/2 - \beta)$ is positive or negative depending on whether the positive magnetic polar region (source) is nearer to the north or the south pole of rotation. Since the observed values of a yield reasonably continuous variations only in the domain $\pi/2 \geq |a - \langle a \rangle|$ (no passage over the central prime vertical), we derive the inequalities $i - \beta \geq 0$ $(\pi/2 - \beta \geq 0)$ or $i + \beta \geq \pi$ $(\pi/2 - \beta < 0)$. Under these conditions, for the a-curve A with $p_0 \fallingdotseq 75°$, equation (12) allows i between $\sim 90°$ and $\sim 46°$ corresponding to values of β between $\sim 75°$ (or $\sim 105°$ for $\pi/2 - \beta < 0$) and $\sim 45°$ (or $\sim 135°$ for $\pi/2 - \beta < 0$). In this range there is a solution $i \fallingdotseq 64°$ and $\beta \fallingdotseq 60°$ very near to the parameters $i = \beta = 60°$ adopted by Böhm-Vitense (1966) in her model calculation. The Böhm-Vitense model has a po-

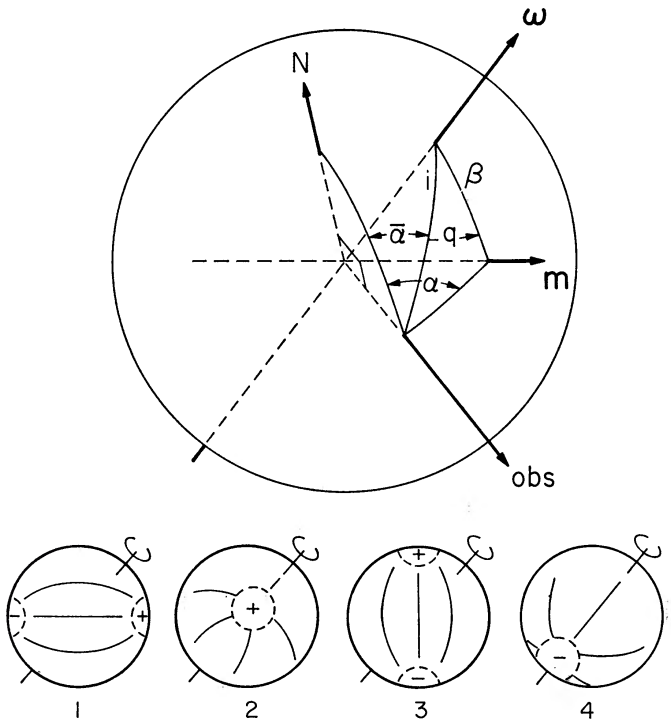

FIG. 8.—Special configurations and parameters of oblique rotator ω, axis of rotation; m, axis of poloidal magnetic field; *obs*, line of sight; N, north. 1, $a = a(\max)$, $E \fallingdotseq 0.9$; 2, $a = \langle a \rangle$, $E \fallingdotseq 0$ 2; 3, $a = \langle a \rangle$ (min), $E \fallingdotseq 0.4$; 4, $a = \langle a \rangle$, $E \fallingdotseq 0.6$. (In the illustration bars are used, instead of angular brackets, to denote averages.)

loidal nondipole magnetic field whose intensity reaches a maximum near the magnetic equator. The parameters determining the angles and distributions were fitted to the variations of the strength of the effective longitudinal field observed by Babcock and Burd (1952). A small variation of parameters will bring the Böhm-Vitense model into agreement with the present data. Her model finds support not only from the coincidence of parameters with these from our probable solution based on the observed magnetic effects, but also from the general agreement of calculated and observed line profiles.

In the case of a rotating star, each point on the stellar surface corresponds to a certain radial velocity, and accordingly to a certain shift of the wavelength. When chemical elements are uniformly distributed, the observed lines have the rotational profile (cf. Unsöld 1955). If chemical elements are not uniformly distributed, lines have irregular profiles with peaks at the wavelengths which correspond to the radial velocities of the regions rich in the elements producing the lines. The variation of line profiles is, therefore, one of the inevitable characteristics of the oblique-rotator models, and a line profile represents a sort of mapping of the distribution of the chemical elements over the rotating stellar surface. In Figure 9, our observed profiles are compared with profiles calcu-

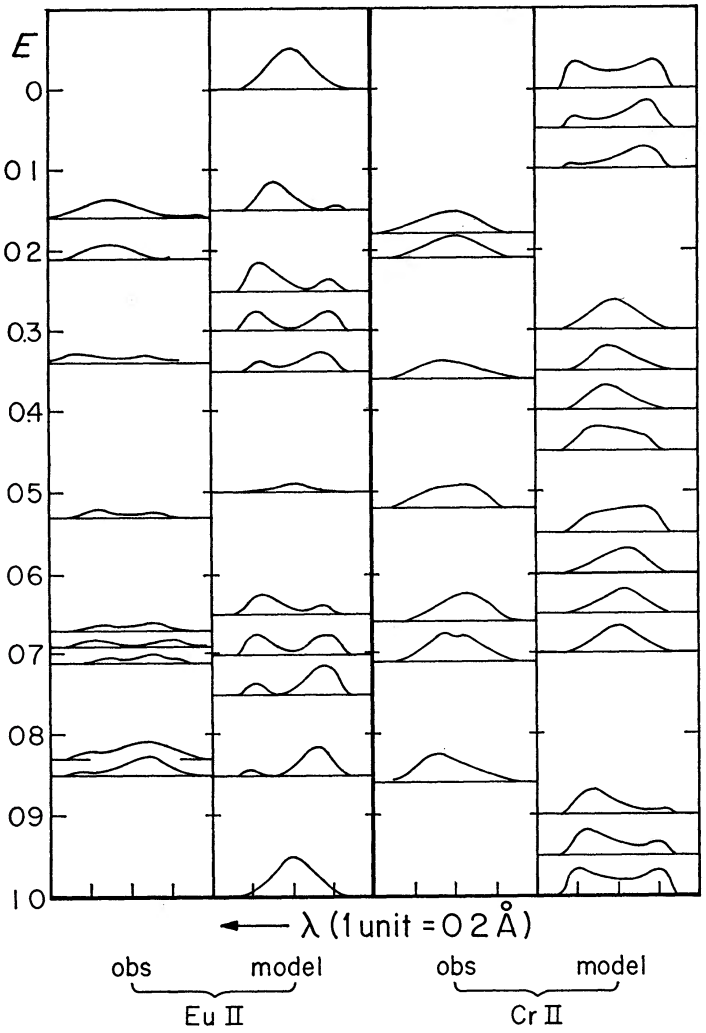

FIG. 9.—Comparison of observed profiles with the predictions by Böhm-Vitense (1966). Ordinate is in approximately linear scale in arbitrary units.

lated by Böhm-Vitense (1966) for her oblique-rotator model ($i = \beta = 60°$) of α^2 CVn. She assumed simple analytic forms for distributions, functions of distance from the magnetic equator only, and fitted the parameters as well as possible to the observed radial velocity and line intensity. In that model Eu II is most abundant at the poles, and Cr II at the equator. The agreement between the predicted and the observed profiles is satisfactory in general, suggesting the validity of the oblique-rotator hypothesis for α^2 CVn. On careful examination, one finds small discrepancies between the compared profiles of Cr II at $E \fallingdotseq 0.7$ and of Eu II at $E \fallingdotseq 0.35$, which are both related to the discrepancies in the radial velocity (see Böhm-Vitense 1966, Figs. 2 and 9). These discrepancies can probably be attributed to small skewnesses in the actual distributions. A further determination of detailed maps, as done by Deutsch (1958) for HD 125248, could reveal more about the relations between the magnetic field and the concentrations of the chemical elements, from which we may eventually infer the physical processes responsible.

The validity of the oblique-rotator hypothesis, however, should not be generalized for all classes of Ap stars; the remarkable spectrum-variable star, HD 221568, for example, was found to be a nonoblique rotator by one of us, Kodaira (1967).

The authors wish to thank the staffs of the Okayama Astrophysical Observatory for their technical assistance, and Naomi K. and Jesse L. Greenstein of the California Institute of Technology for reading the manuscript and giving many valuable suggestions.

REFERENCES

Babcock, H. W. 1951, *Ap. J.*, **114**, 1.
———. 1956, *ibid.*, **124**, 489.
———. 1962, in *Astronomical Techniques*, ed. W. A. Hiltner (Chicago: University of Chicago Press), chap. v.
Babcock, H. W., and Burd, S. 1952, *Ap. J.*, **116**, 8.
Böhm-Vitense, E. 1966, *Zs. f. Ap.*, **64**, 326.
———. 1967, in *Magnetism and Cosmos*, ed. W. R. Hindmarsh *et al.* (New York: American Elsevier Publishing Co.), p. 179.
Burbidge, G. R., and Burbidge, E. M. 1955, *Ap. J. Suppl.*, **1**, 431.
Chandrasekhar, S. 1960, *Radiative Transfer* (New York: Dover Publications), p. 34.
Deutsch, A. J. 1952, *Trans. I.A.U.*, **8**, 801.
———. 1956, *Pub. A.S.P.*, **68**, 92.
———. 1958, *I.A.U. Symp.*, No. **6**, 209.
Farnsworth, G. 1932, *Ap. J.*, **76**, 313.
Kodaira, K. 1967, *Ann. Tokyo Astr. Obs.*, 2d ser., **10**, 157.
Ludendorff, H. von. 1906, *Astr. Nach.*, **173**, 4.
Nishi, K. 1962, *Pub. Astr. Soc. Japan*, **14**, 325.
Stepanov, V. E. 1960, *Astr. Zh.*, **37**, 631 (*Soviet Astr.—AJ*, **4**, 603).
Struve, O., and Swings, P. 1943, *Ap. J.*, **98**, 361.
Unno, W. 1956, *Pub. Astr. Soc. Japan*, **8**, 108.
Unsöld, A. 1955, *Physik der Sternatmosphären* (2d ed., Berlin: Springer-Verlag), p. 515.